POLITECNICO DI TORINO
Repository ISTITUZIONALE

Design and testing of an emergency humanitarian tent for airborne risk mitigation with natural ventilation

Original
Design and testing of an emergency humanitarian tent for airborne risk mitigation with natural ventilation / Gentile, V., Nigra, M., Simonetti, M., Perino, M.. - ELETTRONICO. - 672:(2025). (ROOMVENT 2024 Healthy air together Stockholm April 22-25, 2024) [10.1051/e3sconf/202567201006].

Availability:
This version is available at: 11583/2995256 since: 2024-12-12T14:37:43Z

Publisher:
EDP Science

Published
DOI:10.1051/e3sconf/202567201006

Terms of use:

This article is made available under terms and conditions as specified in the corresponding bibliographic description in the repository

Publisher copyright

(Article begins on next page)

18 November 2026

Design and testing of an emergency humanitarian tent for airborne risk mitigation with natural ventilation

Vincenzo Gentile[1*], *Marianna* Nigra[2], *Marco* Simonetti[1], *Marco* Perino[1]

[1]Energy Department, Politecnico di Torino, C.so Duca degli Abruzzi 24, 10129 Turin, Italy
[2]Interuniversity Dept. Of Regional and Urban Studies and Planning, Politecnico di Torino, Viale Mattioli 39, 10125 Turin, Italy

Abstract. This work presents the methodology and experiments conducted to investigate the impact of natural ventilation in designing an emergency tent that addresses Infection Prevention Control measures against disease transmission via airborne routes. SF6 tracer gas was used to analyze the decay of contaminants within various internal partitions and the indoor space of the emergency treatment module. The study focused on a transparent space partition equipped with medical tools, facilitating emergency interventions without accessing the infected patient area. It aimed to assess the prevention and control of potential airborne transmission across the transparent space partition of the emergency treatment module and to explore the potential role of natural ventilation in limiting or preventing such contamination.

1 Introduction

The World Health Organization (2022) reports that: *'...since 2011, there have been more than 1200 outbreaks of epidemic-prone diseases in 188 countries around the world, causing widespread death and suffering, disproportionately affecting the poorest and most vulnerable populations, and leading to social, economic and political disruption'*. These new diseases established the groundwork for the crucial real-world challenge of promptly providing the medical sector with infrastructure support in emergencies, capable of adhering to appropriate Infection Prevention Control (IPC) measures, upholding environmental principles of sustainability and resilience, and guaranteeing the respect and dignity of individuals and communities [1]. To address this issue, numerous humanitarian organizations, including the United Nations Humanitarian Response Depot (UNHRD), the World Food Programme (WFP [2]), the World Health Organization (WHO [3]), and many more partners, are currently supporting initiatives to encourage the development of efficient products and processes in terms of preparedness and response to address this challenge.

Despite multiple efforts in both the private sector and academia on designing and manufacturing emergency products, new challenges like COVID-19 and emerging airborne diseases push the boundaries of the design requirements of emergency temporary structures. The comprehensive analysis of innovations in transportable healthcare architecture, boosted by the needs that emerged with COVID-19, highlights the gap between market products capable of dealing with control measures related to health emergencies connected to airborne diseases, especially in the humanitarian context [4]. Although the presence of multiple studies in the last twenty years on thermal comfort in humanitarian emergency tents and shelters [5]–[9], only a few focused on the role of natural ventilation contributing to thermal comfort [10] or on the prevention role in the spread of airborne diseases [1][11]. This work focuses, therefore, on the airborne route.

Individuals emit liquid particles through the respiratory system that evaporate quickly and generate bioaerosols. This suspension of small liquid particles (size 1÷100 μm) in the turbulent respiratory cloud [12] can carry a range of pathogens load, depending also on the stage of the disease in the infected individual. Within a short distance from the infected emitter, a susceptible individual may be directly exposed to the respiratory cloud, inhaling particles or capturing them by deposition on its mucosa, leading to potential infection [13][14] [15], [16].

Long-time airborne particles remain suspended [17]. They can diffuse and be transported by airflow, accumulating in an indoor volume if not properly diluted [18]. The pathogens can remain active for a significant time (hours to days) in the aerosol. People can be exposed to pathogens by inhalation via an indirect mechanism, usually called a long-distance transmission route.[19][20], [21]

Ventilation systems and indoor airflow topology can effectively mitigate the spread of pathogens, reducing the exposure of vulnerable people to infectious doses by direct and indirect mechanisms [22]–[30]. Dilution through ventilation and air filtration are common practices to reduce the concentration of indoor airborne particles. Compared to the 7-10 L/s outdoor airflow rate per person recommended by ventilation standards for the no-contagion scenario, when dealing with COVID-19, both the Centers for Disease Control and Prevention (CDC) [23] and the World Health Organization (WHO) [24] recommended ventilation rate up to 160 l/s/patient or at least 12 air changes per hour (ACH) in critical areas such as the Intensive Care Units (ICU).

In contingency pandemic situations, healthcare structures set up as tents can be a valuable resource, alleviating logistics challenges. Tents offer a practical and effective solution for treating infected patients and managing healthcare requirements, especially in remote and impoverished areas. However, access to power and

* Corresponding author: vincenzo.gentile@polito.it

© The Authors, published by EDP Sciences. This is an open access article distributed under the terms of the Creative Commons Attribution License 4.0 (https://creativecommons.org/licenses/by/4.0/).

equipment for ventilation in such contexts may be problematic.

This study presents and analyses an innovative solution for emergency tents.

The design aims to leverage natural ventilation and provides a resilient strategy for handling aerially transmitted diseases.

The dilution effect of natural ventilation in realistic environmental conditions was studied and quantified through tracer decay experiments of the concentration of the gaseous contaminant SF6.

Indoor and outdoor environmental conditions (air temperature, solar radiation, wind velocity, and direction) were continuously monitored during the whole measurement campaign. These quantities are crucial for providing insight into the mechanisms that drive natural ventilation and understanding its impact on infection control. To ensure robust and comparable data collection, experiments were repeated multiple times, examining different scenarios with varying levels of windows opening. A grey-box model was then developed to analyze the results of the tracer gas experiments and assess the number of air changes per hour. The free parameters of the grey-box model were identified by means of a fitting procedure that minimizes the error between the experimental data and the model predictions.

2 The Tent and the specific measures for controlling the spread of infectious diseases

In June 2021, the World Food Programme (WFP) and WHO launched INITIATE²[2], a 5-year initiative that brings together emergency response actors, as well as research and academic institutions, to develop innovative and standardized solutions and related training in support of readiness and response capabilities in health emergencies.

Within this context, the Politecnico of Torino, Italy – with many international institutions and humanitarian organizations – was involved in designing, simulating, and testing an innovative infectious diseases treatment module that could be deployed and utilized in the first phases of health emergencies.

In particular, the work carried out by Politecnico di Torino focused on the role of natural ventilation concerning the prevention and control of possible airborne transmission across internal partitions and in the indoor space of the designed treatment module. The internal space of such module (Fig. 1) is organized in two areas: the infected patient room (also called red zone) and the medical staff space (called green zone), where the air should be contaminant-free. The division between these two spaces relies on a transparent screen, equipped with tools and props (medical inspection gloves, pipes, pockets, et cetera) to allow medical intervention without accessing the red zone with the infected patient. This screen represents a critical interface between patient and medical staff. It was, therefore, critical to explore and assess the possible contamination across the screen and the potential role of natural ventilation in limiting or avoiding such contamination.

This work presents the methodological approach used in supporting the design process from a natural ventilation engineering perspective to share the experience in such an innovative endeavor and discuss the rationale of the approach, methods, pros, cons, and pathways for future research developments and methodological refinements.



Fig. 1.a) The humanitarian tent installed in the testing camp of Brindisi. The installation results from assembling repeatable and symmetrical blocks, generating a multi-room environment. b) Each block has a confined area with a transparent layer, as shown at the bottom. The transparent layer acts as a barrier to separate the area where the patient rests (room #1) from the area devoted to the doctor's operation (room #2).

3 Methodology

3.1 Experimental setup and testing procedure

In order to assess the behavior of the tent in relation to the performance of the natural ventilation and to test the transparent partitioner for the control of infectious diseases, an experimental campaign with tracer gases was done. A specific focus was put on determining the exchange between the two environments since this factor is pivotal in estimating potential risks of cross-infection from the patient to the doctor's room due to airborne transmittable diseases.

Measurements were performed on a real scale prototype (as designed by WHO, Fig. 1a and 1b) installed outdoor in Brindisi (south of Italy).
The main goals were:

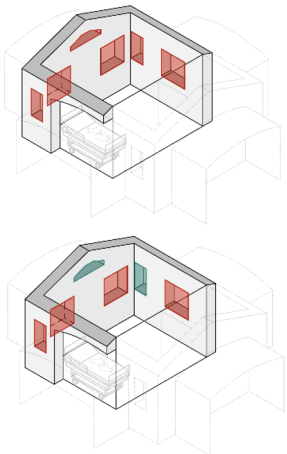
a) to measure the air change rate of the patient room (room #1 – Fig. 2 and 3) and of the doctor's room (room #2 – Fig. 2 and 3),
b) to assess the eventual air exchange between the patients' and the doctors' room. The minimization of these flow rates – $Q_{ex,12}$ and $Q_{ex,21}$, Fig. 3 - avoids cross-contamination risks. All the special measures and solutions taken in the tent design aim to minimize these quantities.

An accurate and reliable assessment of the inter-room air flows (Q_{ex}) would require a technique based on 2 different tracer gases. Moreover, a multi-point sampling would be needed to monitor (over time) the tracer mean concentration in rooms #1 and #2 simultaneously.
However, because the experimental campaign had to be started with very short notice and finished in a few days (the prototype tents were available only briefly), an emergency measurement setup was adopted (no multi-point/multi-gas analyzers were available then).

A suitably modified tracer decay procedure was conceived and performed by conducting a series of SF_6 decay measurements in the patients' and doctors' rooms. Each test was repeated twice (with analogous boundary conditions and identical window configurations – open/close). The first test (Test A) starts by injecting the tracer in the patient room (#1) while monitoring the SF_6 concentration over time in the same room (e.g., #1).
The second test (Test B) follows the conclusion of Test A, still injecting the tracer in the patient room (#1) but monitoring the SF_6 concentration over time in the doctors' room (e.g. #2). At the beginning of each full test (the couple of A and B), the tracer was re-injected (and thoroughly mixed) in room # 1, trying to reach about the same initial gas concentration.
The air change rates and inter-room air flows were estimated by analyzing the coupled time series of the SF_6 concentration detected during Test A and B (e.g., superimposing the two concentration trends) by means of a purposely developed grey-box model.

This approach is a significant stretch concerning a rigorous multi-gas/multi-point procedure, and a non-negligible uncertainty will unavoidably affect the results. However, in this phase of the research (during which the design of the tent and the choice of the components/technical solutions are still under development and are the main goal), it was more important to quickly have an overall draft idea of the performance of the system – even if with a larger interval of confidence – than to gather an accurate picture of the phenomenon (more accurate and reliable tests are planned and will be done).
During the tests, the SF_6 was introduced into the patient's resting area using a 10-liter vessel pressurized at 11 bars, with the injection lasting 10 seconds. It resulted in an initial concentration in the patient room ranging from 120-160 ppm across the various tests.

Concentration measurements of the tracer gas were carried out using the photoacoustic gas monitor Lumasense Innova 1512, equipped with a 16-bit analog/digital converter featuring ±0.25% zero drift, ±0.5% F.S. accuracy on output value, and 1% repeatability on the measured value. Sampling was done by connecting the monitor to a 6 mm nylon tube with four branches, allowing gas sampling at different locations within the same room (to have a reliable lecture on the mean gas concentration in the room).
The experiments (a combination of Test A and B) were repeated multiple times for each scenario to ensure data reproducibility. Figure 2 illustrates the two explored configurations, distinguished solely by varying window openings in the patient room. In the first scenario, all windows remained closed. In the second, two out of six windows were open. The configuration of the doctor's area remained unchanged and confined in both cases.



Scenario 1
Patient room with windows closed. Windows in the doctor's room closed.

Scenario 2
Patient room with open windows in green. Windows in the doctor's room closed.

Fig. 2. Sketches of the patient area (room #1) within each emergency treatment module composing the multi-room environment. The patient room has 6 different windows. In scenario 1, the investigation focuses on natural ventilation with all the windows closed. Differently, in scenario 2 two windows (marked in green) were open.

3.2 Grey-box model for multiroom ventilation

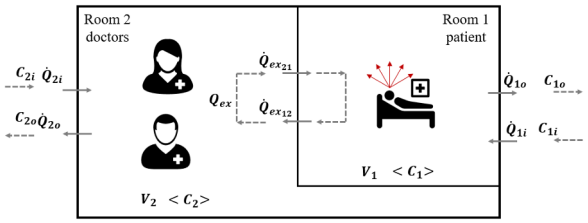


Fig. 3. Scheme of the mass balance of the contaminant (tracer gas SF_6) and the air flows between rooms #1 and #2 and with the outdoor.

In order to assess the outdoor air flows (entering/exiting) in the patient and the doctor's rooms and the interzonal (between rooms #1 and #2) air flow rates, a grey-box model based on the mass conservation of the tracer and of the air, was developed.
The scheme shown in Figure (3), highlights the presence of the following mass flow rates in each room:

- an external mass exchange between the room and the outdoor environment. In particular: Q_1 between room #1 and outdoors, Q_2 between room #2 and outdoors. Subscripts *i* and *o* indicate the inlet or outlet flow for each environment.
- An inter-zonal mass exchange between the two rooms (symbol Q_{ex}. Subscript 12 means from room #1 to room #2. Subscript 21 is the reversed flow).

The mass conservation of the SF_6 written for room #1 and room #2 (in the hypothesis that the air and tracer densities are uniform throughout the two environments) provides:

$$\begin{cases} C_b Q_{1i} + \overline{C_2} Q_{21} - (Q_{10} + Q_{12})\overline{C_1} = V_1 \dfrac{\partial \overline{C_1}}{\partial t} \\ C_b Q_{2i} + \overline{C_1} Q_{12} - (Q_{20} + Q_{21})\overline{C_2} = V_2 \dfrac{\partial \overline{C_2}}{\partial t} \end{cases} \quad (1)$$

In this system, the unknowns are the six air flow rates Q (the trend of the mean room SF_6 concentrations measured and the background concentrations in the outdoor air, C_b, assumed equal to 0).
The full description of the ventilation and the tracer dilution process needs the two mass conservation equations for the air (one for room #1 and one for room #2):

$$\begin{cases} Q_{1i} + Q_{21} - (Q_{10} + Q_{12}) = 0 \\ Q_{2i} + Q_{12} - (Q_{20} + Q_{21}) = 0 \end{cases} \quad (2)$$

The (numerical) solution of these two systems is obtained through a fitting procedure, assuming that the systems of equations (1) and (2) represent a grey-box model of the ventilation mechanism and of the time evolution of the tracer concentration.
The model parameters to be identified are Q_{1i}, Q_{1o}, Q_{12}, Q_{2i}, Q_{2o}, Q_{21}.

3.3 Fitting Procedure

Identifying the grey-box model parameters (Q_{1i}, Q_{1o}, Q_{12}, Q_{21}, Q_{2i}, Q_{2o}) required a fitting procedure of the measured SF_6 concentrations versus time. Specifically, it involves an iterative process utilizing the fitting functions $C_{t1}(Q_{12}, Q_{21}, Q_{10}, Q_{20})$ and $C_{t2}(Q_{12}, Q_{21}, Q_{10}, Q_{20})$, shown in the system (3), to minimize the error function as defined in equation (4). This entails simultaneously computing the total sum of squared differences between each measured concentration (y_i) in rooms #1 and #2 and the corresponding concentration value calculated with the fitting function. (the measured volume of the rooms are: V_1=31.9 m^3 and V_2=21.3 m^3).

$$\begin{cases} C_{t_{i_1}} = C_{t_{i-1_1}} + \dfrac{\Delta t}{V_1}\left[Q_{21} C_{t_{i-1_2}} - (Q_{12} + Q_{10}) C_{t_{i-1_1}}\right] \\ C_{t_{i_2}} = C_{t_{i-1_2}} + \dfrac{\Delta t}{V_2}\left[Q_{12} C_{t_{i-1_1}} - (Q_{21} + Q_{20}) C_{t_{i-1_2}}\right] \end{cases} \quad (3)$$

$$err(C_1, C_2) = \sum_{j=1}^{N}\left[C_{t_{j_1}} - y_j\right]^2 + \sum_{j=1}^{N}\left[C_{t_{j_2}} - y_j\right]^2 \quad (4)$$

The iterative algorithm for minimizing the error function is based on the Generalized Residual Gradient (GRG2) non-linear method, with a residual tolerance of 10^{-8}.
Further, the minimization of the error function in (4) was bounded with a conservation constraint on the volumetric air flow rate in each room derived from the system (2).

4 Results and Discussion

4.1 Experimental Results

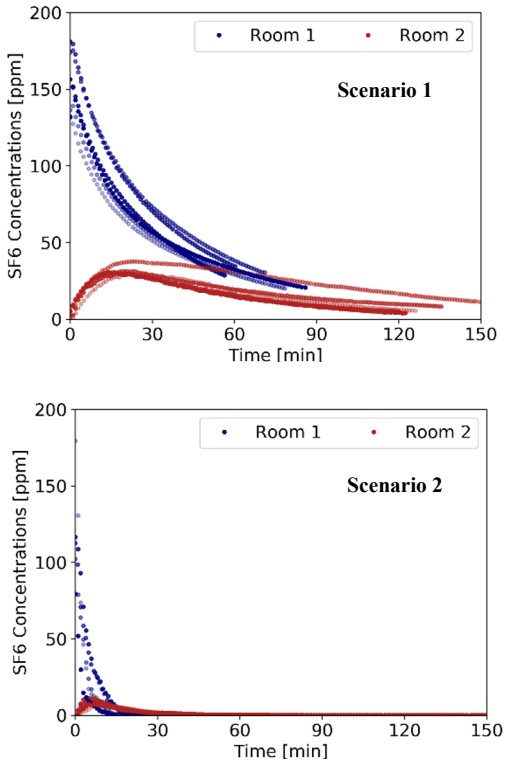


Figure 4. The graph on top depicts the experimental trends of SF_6 concentration in rooms #1 and #2 when the windows in room 1 were closed (scenario 1). On the bottom, the same measurements as when the windows in room #1 without changing room #2 configuration (scenario 2).

Figure 4 shows the two scenarios' coupled tests A and B (A = blue curves, B = red curves) performed. Despite the non-optimal measurement setup (e.g., single-gas, single-point instead of multi-gas, and multi-point), most concentration trends exhibit consistent repeatability for both scenarios, with just a few exceptions. In room #1, where the SF_6 injection happens, a typical exponential decay trend is always found after stopping the injection. In contrast, the trend in room #2 highlights a more complex fluid dynamic behavior. Theoretically, having a perfectly air-tight transparent separating layer between rooms #1 and #2 should mean the absence of tracer gas in the doctor's room. Instead, as clearly shown in Fig. 4, the SF_6 concentration in room #2 follows and "mirrors", with a certain delay, the dynamic of the tracer decay in room #1. In the beginning, the SF_6 concentration rises during the time. Afterward, it starts to follow, with a rather good approximation, an exponential decay. A significant peak of concentration is reached about 20 minutes after the tracer injection in room #1 is stopped. Such a high tracer concentration in the doctor's room indicates a noteworthy airflow exchange between the two spaces, a highly troublesome feature for infection control. It appears quite clear that, despite all the design efforts, the openings in the transparent confinement layer (such as those required for glove usage, patient manipulation, or the passage of wires and tubes

connected to medical equipment) still allow for rather high air exchange between the rooms, thus compromising the confinement of eventual infectious airborne diseases. The time scale of the phenomenon significantly shortens upon opening windows in room #1 (scenario 2). In this case, the contaminant decay duration reduces from over 120 minutes of scenario 1 to less than 30 minutes. The delay at which the concertation peak occurs in room #2 is far shorter, shifting from 20 to 5 minutes after the end of the tracer injection. The peak concentration in the doctor's room is also lower, reducing from about 30 ppm to 15 ppm. Indeed, the window openings, which promote more sustained natural ventilation, help keep the contaminants low and reduce the risk of infection.

4.2 Fitting with the multiroom grey-box model

The six unknown ventilation flow rates were identified by following the procedure highlighted in sections 3.2 and 3.3. Once the model parameters have been assessed, the grey-box model was also used as a simulation tool. Figures 5 and 6 show an example of comparing the measured and predicted concentration-time profiles.

Thanks to the greater number of measured points collected during scenario 1 (that tracer decay lasted longer), the agreement between numerical and experimental data is quite remarkable (e.g., Figure 5 chart on the left). The faster decay of the tracer concentration during scenario 2 reduced the number of available points for fitting roughly to half. This aspect slightly worsens the fitting quality. Figure 6 displays higher approximation errors, particularly after 20 minutes from stopping the tracer gas injection and at very low SF_6 concentration levels. Operating within a lower concentration range reduces the accuracy of the sampling apparatus, heightening data uncertainty. For scenario 2, the fitting function still reasonably approximates the concentration trends, unveiling a tenfold increase in exchanged flow rates (e.g., Figure 6 chart on the left).

Concerning the values of the airflow rates identified using the fitting procedure (shown in Figures 5 and 6 on the right-hand side chart), it is possible to see the following.

For Scenario 1: on average, the inter-zonal airflow rate from room #1 to room #2 (Q_{12}) was 27.9 m^3/h. Considering all the various repeated measurements done with this window configuration, the Q_{12} ranged from about 20 to 40 m^3/h. Because the volume of room #2 is 21.3 m^3, the volumetric air change rate, potentially carrying airborne biological contaminants, ranges from 0.94 to 1.9 1/h. It is an unexpected result since this flow rate is rather high, while the design expectations suggested a negligible air exchange between the doctors' and patients' rooms. Nonetheless, the adverse effects of this high flow rate are partially balanced by a more effective dilution due to a higher fresh air entering room #2 (Q_{2i} = 64.8 m^3/h). It is worth noting how the fresh air flow rate from the outdoors into the patient room (Q_{1i}) is practically zero, and the exhaust air flow rate (Q_{1o}) is almost equal to the interzonal air flow from rooms #1 and #2. It means that, in practice, the ventilation of the patient room happens entirely thanks to the air from room #2 (Q_{21} = 64.8 m^3/h).

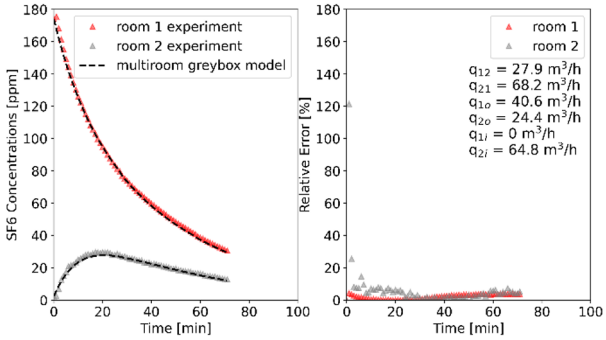


Fig. 5. Example of fitting results from the combination of tests A and B for scenario 1. The comparison between experimental results (dashed line) and the multiroom grey-box model is on the left. The relative errors from the fitted and corresponding measured values are on the right.

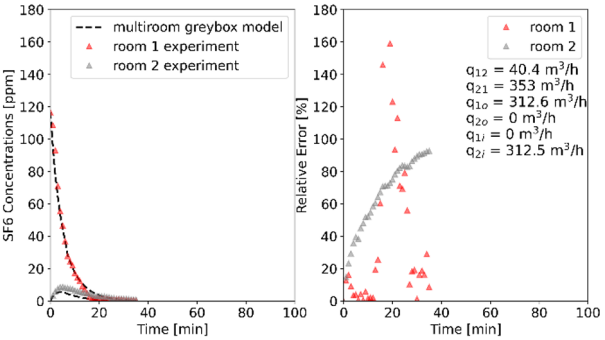


Fig. 6. Example of fitting results from the combination of tests A and B for scenario 2. The comparison between experimental results (dashed line) and the multiroom grey-box model is on the left. The relative errors from the fitted values and the corresponding measured values are on the right.

For Scenario 2: A comparison between figures 5 and 6 reveals comparable absolute values of the inter-zonal air flow rate from room #1 to room #2 (on average, the inter-zonal airflow rate from room #1 to room #2 - Q_{12} - was 40.4 m^3/h). On the contrary, significant variations are shown regarding the exchange rates between rooms and the outdoors. Specifically, the fresh air entering into room #2 (Q_{2i} = 312.5 m^3/h) and the outflow from room #1 (Q_{1o} = 312.6 m^3/h). Moreover, there is a substantial shift in the flow pattern, with higher internal airflows from room #2 to room #1 (Q_{21} = 353.0 m^3/h). This airflow configuration is especially advantageous when handling patients potentially transmitting infections through the air. Indeed, a structure with airflows that are about 9 times higher from room #1 to room #2 and vice versa results in a safer condition, mitigating the risk of transmission for doctors during emergency operations.

However, it has to be noted that, depending on the wind direction/speed and/or indoor-outdoor temperature difference, the airflow path may reverse its direction. Again, it is confirmed a poorer performance than expected for the transparent separating layer regarding air tightness (the design assumptions were to realize the best separation possible, e.g., air tightness, between rooms #1 and #2).

Finally, the improvement of the natural ventilation due to the window opening in the patient room led to an increase in the fresh air flow rate (the air change per hour rises from around 1 of scenario 1 to 10 1/h) in both the rooms and assured a better dilution of contaminants.

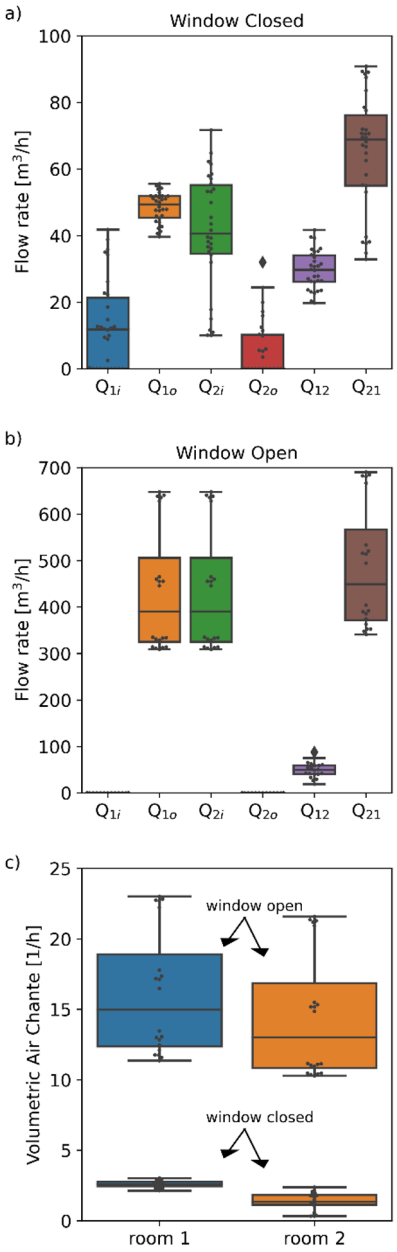


Fig. 7. Three graphs indicating the air flow rate values identified with the grey-box model. The 6 air flow rates were identified for each experiment, and their range of variation (among the various tests) is shown as a box plot. (a) = Scenario 1, (b) = Scenario 2. In (c), the estimated air changes per hour variation for rooms #1 and #2 is plotted.

The complete experimental activity spanned two days to gather comprehensive data across various scenarios. In total, 6 experiments were performed for scenario 1 with analogous boundary conditions and 4 experiments for scenario 2. Figure 7 summarizes the variation of the model parameters identified for each repeated test.

The top graph (Fig. 7a), related to scenario 1 - with closed windows - shows a marginal fluctuation in the fitted flow rates, aligning with slight variations in outdoor conditions such as temperature and wind velocity throughout the day. Minor temperature and air velocity shifts between different tests might account for the fluctuations in values observed. Indeed, the relative pressure difference between the two rooms is influenced by those variables, inducing the variation in airflow rate values and increasing the data sparsity. However, in the second scenario (Fig. 7b) the impact of external distrurbants on the flow rate values can be lower because the higher average values. Consequently, fitted values have a reduced sparsity, and data are more concentrated around the median.

Finally, Fig.7c shows the related volumetric air change in the two rooms and each scenario. The value is calculated considering all the *"fresh"* entering flows in each room, as in the following equations:

$$n_{room\ 1} = \frac{Q_{1i} + Q_{21}}{V_1} \quad (5)$$

$$n_{room\ 2} = \frac{Q_{2i}}{V_2} \quad (6)$$

We used this definition, associating the concept of fresh air with the possible presence of pathogenic contaminants. Therefore, for room 1, the airflow entering from room 2 also contributes to increased ventilation. On the contrary in room 2, because the air entering from room 1 can potentially carry out pathogens emitted from the patient, is not included in the definition of volumetric air change.

The increase of ventilation, induced by the partial opening of windows, realized an increase of one order of magnitude in the air change of both rooms (from values between 1-4 1/h to 10-22 1/h) and helped to match indications provided by CDC [23] and WHO [24].

5 Conclusion

This paper presented research activities concerning the design, development and test of an emergency tent integrating innovative features tailored to handle airborne diseases efficiently. Our focus was to establish resilient strategies capable of handling airborne transmission risks. Two major measures were pivotal: leveraging natural ventilation and installing a purposely built transparent separation layer between the patient's and the doctor's spaces.

Initially, our efforts concentrated on supporting the design and optimization of natural ventilation strategies by providing information about the shape, size, and locations of ventilation openings/windows. Once a real-scale prototype was conceived and built, the research focused on testing the tent's actual performance. Tracer gas techniques were employed to evaluate the effectiveness of natural ventilation and the transparent separating layer in mitigating the risk associated with airborne contaminants.

Because of the intricate configuration of the system with interconnected rooms with complex ventilation airflow paths, and given the necessity of performing the experiments with short notice and within a few days, a

purposely methodology was developed and applied. It involved conducting two sequential tracer decay tests, injecting the tracer always in the same room and sequentially monitoring the time evolution of the tracer concentration, one time in one room and the second time in the other room.

Utilizing a grey-box model, we identified all the relevant air flow rates exchanged between the rooms and outdoors, as well as the inter-zonal exchanges. The multiroom grey-box model consists of four conservation equations: two related to the tracer gas concentration and two to the ventilation air. The model parameters are then identified by best-fitting the experimental data of the tracer concentration.

Although the simplicity of this approach it provided pivotal insights essential for optimizing the emergency treatment module, particularly enhancing the design of the transparent partitioning layer. The proposed experimental technique and the procedure for analyzing the tracer gas data demonstrated the capability to provide reliable and repeatable results. The insight offered by the outcomes of the tracer gas analysis allowed us to determine an overall picture of the natural ventilation strategies' performance and the transparent separation layer.

In particular, analyses confirmed that adopting natural ventilation concepts in emergency hospitals can significantly help reduce the risk of cross-infection. For example, in scenario 2, a significant airflow from the doctor's room toward the patients room assures a safer doctor's environment. Yet, it is also important to mention that climatic and geographic conditions might drastically influence the degree of effectiveness of natural ventilation in the emergency context, both in terms of comfort and infection prevention control. Wind direction/speed and the indoor/outdoor temperature difference can potentially change the airflow path in size and direction, thus jeopardizing the containment of the pathogens.

A quite unexpected result was finding non-negligible air flow rates between rooms #1 and #2 (e.g., patient and doctor's room) for all the tested boundary conditions. This is a clear indication that the design and construction of the transparent partitioning layer still need major improvements.

While our experimental methodology offered valuable insights, acknowledging its limitations is crucial. Indeed, a multi-tracer technique with multi-point sampling probes would provide more reliable and accurate results. On the other hand, the simplified approach allowed us to perform the experiments using very simplified hardware and in a very "agile" way. Features conceived to address time constraints and execution speed are mandatory, especially when assessing real environment tests. Additionally, the simplicity and robustness of the instruments and the experimental setup are at a premium, especially when assessing experimental activities outside optimal environments such as labs or testing chambers.

The introduced simplifications affect the accuracy of results, whose effects are - for now - not exactly quantifiable. Acknowledging these drawbacks, further development of this research is planned. Firstly, a more reliable measurement technique (using two tracer gases and multi-point sampling) will be developed, set up, and used in the near future. Moreover, tracer gas decay can be very quick due to the high ventilation air flow rates when windows are partially or totally open. This feature can become serious if a traditional gas monitor (like the photoacoustic gas monitor Lumasense Innova 1512) is adopted due to the long acquisition time (1 minute per measured point).

Consequently, only a few points are detectable with fast decay trends, translating into poor and less accurate fitting results caused by the poor availability of data. Adopting a new measurement apparatus based on fast response sensors and low-cost electronic boards allowing a multi-gas/multi-point approach is under development. Furthermore, our upcoming endeavors aim to sample tracer gases across various room points to detect local and mean concentration values, allowing for a more detailed and precise assessment of airflow paths and rates within the different sections of the tent.

References

[1] M. Nigra, A. Silenzi, and M. Di Marco, "What Do an Anaesthesiologist, a Nurse, Two Designers, and a Professor in Architectural Technology Do Together in a Room? Crafting Interdisciplinarity As Response To Emerging Infectious Diseases," *Proc. Des. Soc.*, vol. 3, no. July, pp. 3871–3878, 2023, doi: 10.1017/pds.2023.388.

[2] "The World Health Organization (2022), INITIATE2. WHO."

[3] "The World Health Organization (2022), Health Emergencies. WHO."

[4] Stephen Verderber, *Innovations in Transportable Healthcare Architecture*, 1st Editio. London, 2015. doi: https://doi.org/10.4324/9781315684550.

[5] C. Crawford, P. Manfield, and A. McRobie, "Assessing the thermal performance of an emergency shelter system," *Energy Build.*, vol. 37, no. 5, pp. 471–483, 2005, doi: 10.1016/j.enbuild.2004.09.001.

[6] C. Cornaro, D. Sapori, F. Bucci, M. Pierro, and C. Giammanco, "Thermal performance analysis of an emergency shelter using dynamic building simulation," *Energy Build.*, vol. 88, pp. 122–134, 2015, doi: 10.1016/j.enbuild.2014.11.055.

[7] D. Albadra, M. Vellei, D. Coley, and J. Hart, "Thermal comfort in desert refugee camps: An interdisciplinary approach," *Build. Environ.*, vol. 124, pp. 460–477, 2017, doi: 10.1016/j.buildenv.2017.08.016.

[8] A. Ullal *et al.*, "Comparing thermal performance of standard humanitarian tents," *Energy Build.*, vol. 264, pp. 1–11, 2022, doi: 10.1016/j.enbuild.2022.112035.

[9] P. Manfield, J. Ashmore, and T. Corsellis, "Design of humanitarian tents for use in cold climates," *Build. Res. Inf.*, vol. 32, no. 5, pp. 368–378, 2004, doi:

10.1080/0961321042000220990.

[10] M. Hamdan, F. Abd-Alhamid, and L. Dabbour, "Impact of passive techniques on thermal behavior of emergency shelters," *Ecol. Eng. Environ. Technol.*, vol. 22, no. 3, pp. 112–119, 2021, doi: 10.12912/27197050/135523.

[11] N. Bagdasarian *et al.*, "A safe and efficient, naturally ventilated structure for COVID-19 surge capacity in Singapore," *Infect. Control Hosp. Epidemiol.*, vol. 42, no. 5, pp. 630–632, 2021, doi: 10.1017/ice.2020.309.

[12] L. Bourouiba, "Fluid dynamics of respiratory infectious diseases," 2021.

[13] T. Asai, E. Kurosaki, K. Kimachi, M. Nakayama, and M. Koido, "Peak risk of SARS - CoV - 2 infection within 5 s of face - to - face encounters : an observational / retrospective study," *Sci. Rep.*, no. 0123456789, pp. 1–9, 2023, doi: 10.1038/s41598-023-44967-x.

[14] L. Morawska, G. Buonanno, A. Mikszewski, and L. Stabile, "The physics of respiratory particle generation, fate in the air, and inhalation," *Nat. Rev. Phys.*, 2022, doi: 10.1038/s42254-022-00506-7.

[15] W. Chen, H. Qian, N. Zhang, F. Liu, L. Liu, and Y. Li, "Extended short-range airborne transmission of respiratory infections," *J. Hazard. Mater.*, vol. 422, no. June 2021, p. 126837, 2022, doi: 10.1016/j.jhazmat.2021.126837.

[16] W. Chen, N. Zhang, J. Wei, H.-L. Yen, and Y. Li, "Short-range airborne route dominates exposure of respiratory infection during close contact," *Build. Environ.*, vol. 176, p. 106859, 2020.

[17] X. Xie, Y. Li, A. T. Y. Chwang, P. L. Ho, and W. H. Seto, "How far droplets can move in indoor environments - revisiting the Wells evaporation-falling curve," *Indoor Air*, vol. 17, no. 3, pp. 211–225, 2007, doi: 10.1111/j.1600-0668.2007.00469.x.

[18] A. Rahmani *et al.*, "Duration of SARS-CoV-2 shedding and infectivity in the working age population: a systematic review and meta-analysis," *Med. del Lav.*, vol. 113, no. 2, pp. 1–14, 2022, doi: 10.23749/mdl.v113i2.12724.

[19] L. C. Marr and J. W. Tang, "A Paradigm Shift to Align Transmission Routes with Mechanisms," *Clin. Infect. Dis.*, vol. 73, no. 10, pp. 1747–1749, 2021, doi: 10.1093/cid/ciab722.

[20] J. W. Tang, Y. Li, I. Eames, P. K. S. Chan, and G. L. Ridgway, "Factors involved in the aerosol transmission of infection and control of ventilation in healthcare premises," *J. Hosp. Infect.*, vol. 64, no. 2, pp. 100–114, 2006, doi: 10.1016/j.jhin.2006.05.022.

[21] S. Balachandar, S. Zaleski, A. Soldati, G. Ahmadi, and L. Bourouiba, "Host-to-host airborne transmission as a multiphase flow problem for science-based social distance guidelines," *Int. J. Multiph. Flow*, vol. 132, 2020, doi: 10.1016/j.ijmultiphaseflow.2020.103439.

[22] G. Buonanno *et al.*, "Link between SARS-CoV-2 emissions and airborne concentrations: Closing the gap in understanding," *J. Hazard. Mater.*, vol. 428, p. 128279, 2022, doi: 10.1016/j.jhazmat.2022.128279.

[23] GAEF, "Who is the Gesellschaft für Aerosolforschung ? Gesellschaft für Aerosolforschung," no. December, 2020.

[24] N. Zhang *et al.*, "Evidence for lack of transmission by close contact and surface touch in a restaurant outbreak of COVID-19," *J. Infect.*, no. xxxx, 2021, doi: 10.1016/j.jinf.2021.05.030.

[25] Z. T. Ai and A. K. Melikov, "Airborne spread of expiratory droplet nuclei between the occupants of indoor environments: A review," *Indoor Air*, vol. 28, no. 4, pp. 500–524, 2018, doi: 10.1111/ina.12465.

[26] W. Su *et al.*, "Infection probability under different air distribution patterns," *Build. Environ.*, vol. 207, no. PB, p. 108555, 2022, doi: 10.1016/j.buildenv.2021.108555.

[27] Z. Peng and J. L. Jimenez, "Exhaled CO2as a COVID-19 infection risk proxy for different indoor environments and activities," *Environ. Sci. Technol. Lett.*, vol. 8, no. 5, pp. 392–397, 2021, doi: 10.1021/acs.estlett.1c00183.

[28] A. K. Melikov, Z. T. Ai, and D. G. Markov, "Intermittent occupancy combined with ventilation: An efficient strategy for the reduction of airborne transmission indoors," *Sci. Total Environ.*, vol. 744, no. 2, 2020, doi: 10.1016/j.scitotenv.2020.140908.

[29] L. D. Knibbs, L. Morawska, S. C. Bell, and P. Grzybowski, "Room ventilation and the risk of airborne infection transmission in 3 health care settings within a large teaching hospital," *Am. J. Infect. Control*, vol. 39, no. 10, pp. 866–872, 2011, doi: 10.1016/j.ajic.2011.02.014.

[30] S. Deng, J. Lau, P. Wargocki, and Z. Wang, "Associations between Illness-Related Absences and Ventilation and Indoor Pm2.5 in Elementary Schools of the Midwestern United States," *SSRN Electron. J.*, p. 107944, 2022, doi: 10.2139/ssrn.4308051.